

The Stellar Halo in the Inner Milky Way: Predicted Shape and Kinematics

Angeles Pérez-Villegas¹ , Matthieu Portail¹ and Ortwin Gerhard¹

¹ *Max-Planck-Institut für Extraterrestrische Physik, Gießenbachstraße, D-85741 Garching, Germany*

Submitted 4 July 2016

ABSTRACT

We have used N-body simulations for the Milky Way to investigate the kinematic and structural properties of the old metal-poor stellar halo in the barred inner region of the Galaxy. We find that the extrapolation of the density distribution for bulge RR Lyrae stars, $\rho \sim r^{-3}$, approximately matches the number density of RR Lyrae in the nearby stellar halo. We follow the evolution of such a tracer population through the formation and evolution of the bar and box/peanut bulge in the N-body model. We find that its density distribution changes from oblate to triaxial, and that it acquires slow rotation in agreement with recent measurements. The maximum radial velocity is $\sim 15 - 25$ km/s at $|l| = 10^\circ - 30^\circ$, and the velocity dispersion is ~ 120 km/s. Even though the simulated metal-poor halo in the bulge has a barred shape, just 12% of the orbits follow the bar, and it does not trace the peanut/X structure. With these properties, the RR Lyrae population in the Galactic bulge is consistent with being the inward extension of the Galactic metal-poor stellar halo.

Key words: Galaxy: bulge – Galaxy: Kinematics and dynamics – Galaxy: structure – Galaxy: centre – methods: numerical

1 INTRODUCTION

The inner region of the Milky Way (MW) hosts multiple components such as the bar and box/peanut (B/P) bulge, the thin and thick disks, and the inner stellar halo. Stars in the Galactic bulge thus occupy a wide range in the Metallicity Distribution Function (MDF), with $[\text{Fe}/\text{H}]$ between -3.0 and $+1.0$ dex (Rich 1988; Zoccali et al. 2003; Ness et al. 2013a; Gonzalez et al. 2015).

In the bulge region of the Galaxy a small but not insignificant fraction of metal-poor stars has been detected. About 5% of the ARGOS sample (Ness et al. 2013a) have metallicities $[\text{Fe}/\text{H}] < -1.0$. These metal-poor stars show a slower rotation and a higher velocity dispersion than the stars with metallicity $[\text{Fe}/\text{H}] > -1.0$ (Ness et al. 2013b). Their different kinematics is possible evidence that the metal-poor bulge stars are not part of the B/P bulge, but belong to a distinct component. Other studies conclude that the MDF in the bulge can be separated into a metal-rich population of stars that are part of the B/P bulge, and a metal-poor population that traces an old spheroidal component (Babusiaux et al. 2010; Hill et al. 2011; Rojas-Arriagada et al. 2014).

RR Lyrae stars (RRLs) are well-known tracers of old,

metal-poor populations, and have been used to trace the old component in the Galactic bulge. The bulge RR Lyrae population has a MDF centered around $[\text{Fe}/\text{H}] = -1.0$, with a small spread in metallicity (Walker & Terndrup 1991; Pietrukowicz et al. 2012). Thousands of RRLs have been discovered in the bulge (Soszyński et al. 2011, 2014), and these stars are ideal tracers of structures because their distances can be accurately estimated. However, there is disagreement on the spatial distribution of the bulge RRLs: Dékány et al. (2013) find that the RRL distribution is spheroidal with a slight elongation inside 1 kpc, whereas, Pietrukowicz et al. (2015) find that the spatial distribution of RRLs is barred, but that the RRLs are not part of the X-shaped structure seen in red clump giant stars (e.g. Wegg & Gerhard 2013). The old RRL component in the bulge could represent the inner extension of the Galactic halo (Alcock et al. 1998; Minniti et al. 1999) even though it is barred, due to gravitational effects of the bar that formed later in the disk (Saha et al. 2012). A recent radial velocity (RV) study in the inner bulge ($|l| < 4^\circ$) has shown that the RRL rotate slowly if at all (Kunder et al. 2016).

Combining these new data, detailed studies can now be made of the properties of the stellar halo in the inner region around the Galactic bar. The questions that we want to address in this study are: Could the metal-poor stars in the bulge be part of the inner stellar halo? What is the in-

* E-mail: mperez@mpe.mpg.de

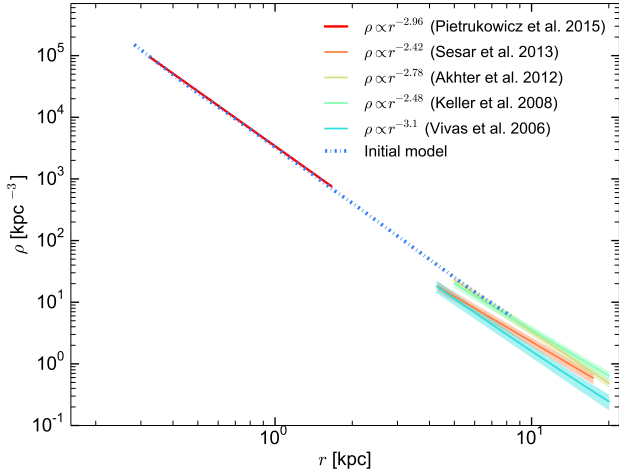


Figure 1. RRL spatial density profiles as function of spherical radius. The red solid line shows the deprojected density profile for bulge RRLs determined from the surface density profile given in Pietrukowicz et al. (2015). The coloured solid lines between $\sim 5 - 20$ kpc radius show the density profiles of stellar halo RRLs from the studies indicated, the shaded areas show the 1σ errors. The dotted line is the stellar halo density profile of the initial model described in Section 3.

fluence of the bar and B/P bulge on the kinematics and spatial distribution of these stars? We use N-body simulations to address these questions because they are powerful tools to study bars and bulges in the evolution of galaxies (Combes et al. 1990; Athanassoula & Misiriotis 2002; Debattista et al. 2006), and similarly the bulge/bar region of the MW (Fux 1997; Sevenster et al. 1999; Shen et al. 2010; Martinez-Valpuesta & Gerhard 2011; Portail et al. 2015a). In this paper, Section 2 discusses the density profile of MW RRLs. Section 3 describes the N-body method that we use for modelling the stellar halo in the bar region. Our predictions for the shape and kinematics of the inner stellar halo are presented in Section 4. Section 5 contains an orbital analysis of the stellar halo particles. Our conclusions are presented in Section 6.

2 DENSITY PROFILE OF RRLS

The density profile of the RRLs in the stellar halo between radii of $5 - 20$ kpc is often described as a single power law, $\rho \sim r^\alpha$, with slope α between -2.4 and -3.1 (Wetterer & McGraw 1996; Amrose & McKay 2001; Vivas & Zinn 2006; Keller et al. 2008; Jurić et al. 2008; Akhter et al. 2012; Sesar et al. 2013). Could the bulge RRL be the inner extension of the RRL halo?

Figure 1 shows the deprojected density profile of bulge RRLs¹ calculated from the surface density profile given by Pietrukowicz et al. (2015) as function of spherical radius r , defined for a triaxial model as $r = \sqrt[3]{abc}$, if a, b, c are the axis lengths of the given isodensity contour. The density profile of the bulge RRLs is well described by a power law with a $\alpha \sim -2.96$ in the distance range between $0.2 - 2.8$

kpc. Also shown in Fig. 1 are density profiles for stellar halo RRLs from the literature, for radii between $\sim 5 - 20$ kpc. We see that if we extrapolate the power-law density profile for the bulge RRLs to larger radii, it matches the density normalizations of the halo RRLs within a factor ~ 2 . Based on this argument, bulge and stellar halo RRLs could be part of the same component.

We note that the MDF of the bulge RRLs has a peak at $[\text{Fe}/\text{H}] = -1.0$ (Pietrukowicz et al. 2015) whereas the halo RRL population peaks at $[\text{Fe}/\text{H}] = -1.4$ (Jurcsik & Kovacs 1996; Nemec et al. 2013; Torrealba et al. 2015). In our interpretation, this implies a metallicity gradient in the bulge-halo RRL population. This could arise, for example in an accretion model for the halo, because the fragments that reached the centre of the MW were chemically somewhat more evolved than those that contributed most of the stars near the Sun. Further information about the history of the halo could be provided by the α -enhancement. For RRLs in the halo $[\alpha/\text{Fe}] \sim 0.3$ dex (Nissen & Schuster 2010; For et al. 2011), however for RRLs in the bulge there are no measurements of $[\alpha/\text{Fe}]$ available in the literature yet. In future, it will be interesting to compare such measurements with the halo RRLs.

Therefore, henceforth we will consider the hypothesis that the RRLs in the bulge are the inner extension of the stellar halo.

3 STELLAR HALO MODEL: N-BODY SIMULATION

We assume that the metal-poor halo traced by RRLs formed early in the history of the MW before the Galactic bar was present. At these early times, we model the stellar halo as an oblate component with axial ratios $b/a = 1.0$, $c/a = 0.6$ and a single power-law density profile $\rho \sim m^{-3}$, where $m = \sqrt{x^2 + \left(\frac{y}{b/a}\right)^2 + \left(\frac{z}{c/a}\right)^2}$. The assumed flattening is consistent with values observed near the Sun (Morrison et al. 2000; Siegel et al. 2002; Chen et al. 2001; Phleps et al. 2005; Sesar et al. 2013) and the normalization is chosen to agree with the bulge RR Lyre profile in Fig. 1. This model is shown by the dotted line in Fig. 1.

To follow the stellar halo through the bar and buckling evolution of the MW, we use the N-body simulation M85 from Portail et al. (2015a) as it evolves in its self-consistent potential $\Phi(\mathbf{x}, t)$, from the initial time ($t = 0$) through bar formation (1.6 Gyr) and buckling (2.8 Gyr) to its final time (5.2 Gyr). We use all the dark matter halo particles from model M85 as test particles which now will be representing the stellar halo. The dark matter particles now have two weights, the first is to calculate the dark matter potential, and the second is the weight that orbits have in the stellar halo. We determine the stellar halo weights using the Made-to-Measure method (Syer & Tremaine 1996; de Lorenzi et al. 2007), such that at $t = 0$ they represent our oblate power-law density model for the stellar halo in $\Phi(\mathbf{x}, t = 0)$. Then at any later time t we can use these same particle weights to determine the properties of the stellar halo in the evolved $\Phi(\mathbf{x}, t)$. Note that our initial stellar halo does not rotate, and has a mild radial anisotropy.

¹ This corrects the normalization in eq. (17) of Pietrukowicz et al. (2015).

4 PREDICTED SHAPE AND KINEMATICS OF THE INNER STELLAR HALO

Now we use the halo particle weights to reconstruct the stellar halo at the final time of the simulation, thereby predicting the shape of its density distribution and the kinematics of the halo stars after several Gyr of gravitational interaction with the bar and B/P bulge.

4.1 Shape of the stellar halo

Figure 2 shows that during the evolution, the shape of the stellar halo in the inner 5 kpc of the Galaxy has changed from the initial oblate distribution with constant axial ratio (left panels) to a triaxial distribution (right panels). At the final time, the axial ratios of the triaxial stellar halo both increase with major axis radius, from ~ 0.6 to 1.0 in b/a , and from ~ 0.5 to ~ 0.7 in c/a . The largest effects of the gravitational influence of the Galactic bar and B/P bulge are seen in the central 3 kpc. The final density profile, in oblate shells with flattening $c/a=0.6$, is similar to the initial stellar halo density as shown in Figure 2, although slightly steeper inside ~ 0.6 kpc.

4.2 Kinematic Maps

We construct time-smoothed kinematic observables for the stellar halo model in the inner Galaxy (see Portail et al. 2015a). Figure 3 shows the predicted kinematics maps for the two snapshots $t = 0$ (top panels) and at the final time (bottom panels). Before bar formation, the mean RV is approximately zero (the model does not initially rotate), and the velocity dispersion is in the range ~ 70 to 110 km/s, depending on galactic longitude and latitude, (l, b) . At the final time, the mean RV is $\sim 15 - 25$ km/s at $|l| = 10^\circ - 30^\circ$ and $|b| \leq 10^\circ$, and the dispersion is ~ 120 km/s outside the central few degrees. The measured rotation in the later stages of the N-body simulation is due to angular momentum transfer mostly during bar formation (Saha et al. 2012). Note that exact values are model-dependent, however, the main point is that the rotation is small compared to that of the B/P bulge.

New kinematic data of the RRLs from Kunder et al. (2016) show that the RR Lyrae stars in the Galactic bulge at $|l| = 4^\circ$, $b \sim -4^\circ$ exhibit hot kinematics with almost negligible rotation. In the right panel of Figure 3, we present the radial velocity distribution of our model versus their data, showing that although the predicted rotation is ~ 6 km/s smaller, the RV histogram is in good agreement with the observations.

On the other hand, the metal-poor stars ($[\text{Fe}/\text{H}] < -1.0$) in the ARGOS survey rotate faster (Ness et al. 2013b) than both our halo model and the bulge RRLs. This could be caused by a contamination of the ARGOS metal-poor component with metal-poor thick disk stars, or by a larger initial rotation of the ARGOS metal-poor stars (as we have checked by suitable models), but in any case the metal-poor halo component that we are discussing here must be different from the ARGOS metal-poor stars.

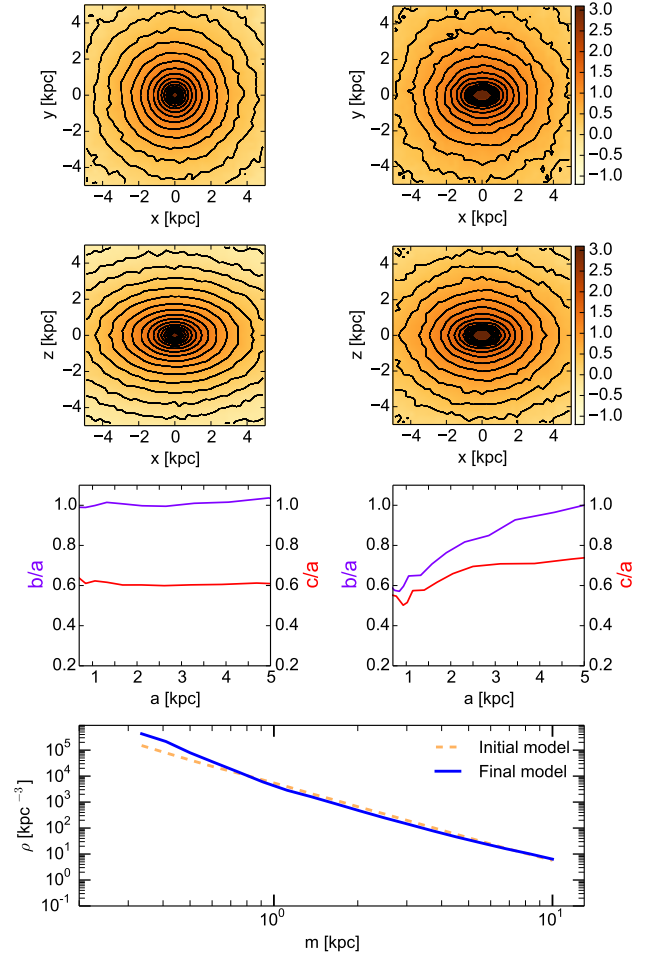


Figure 2. Logarithmic surface density contours of the model stellar halo seen face-on (first row) and side-on (second row). The third row of panels shows the halo axis ratios b/a (purple line) and c/a (red line) as function of the major axis radius a . The initial oblate distribution ($c/a = 0.6$, left) has changed into a triaxial configuration with varying axis ratios at the final time (right). The bottom panel shows the density profile of the model at the initial and final times.

5 ORBITAL ANALYSIS

Our stellar halo model has a bar shape in the inner Galaxy. However, the rotation of this component is slow compared with stars in the Galactic bar and B/P bulge. To understand the kinematic differences between both structures we analyze the halo orbits. To do so, we use frequency analysis. First, we compute the Fast Fourier Transform (FFT) for particle tracks in major axis coordinate x and cylindrical radius R , in order to identify the respective main frequencies. Then we separate the stellar halo particles into bar-following particles, for which the ratio of $f_R/f_x = 2 \pm 0.1$, and not-bar-following particles, with $f_R/f_x \neq 2 \pm 0.1$. We are using the same criteria to classify orbits as Portail et al. (2015b).

For a sample of 30000 stellar halo particles within 5 kpc radius, we find that just 12% of the halo particles follow the bar and 88% do not. In Figure 4, we show the surface density and RV maps on the sky for the entire sample, the bar-following particles, and the not-bar-following particles.

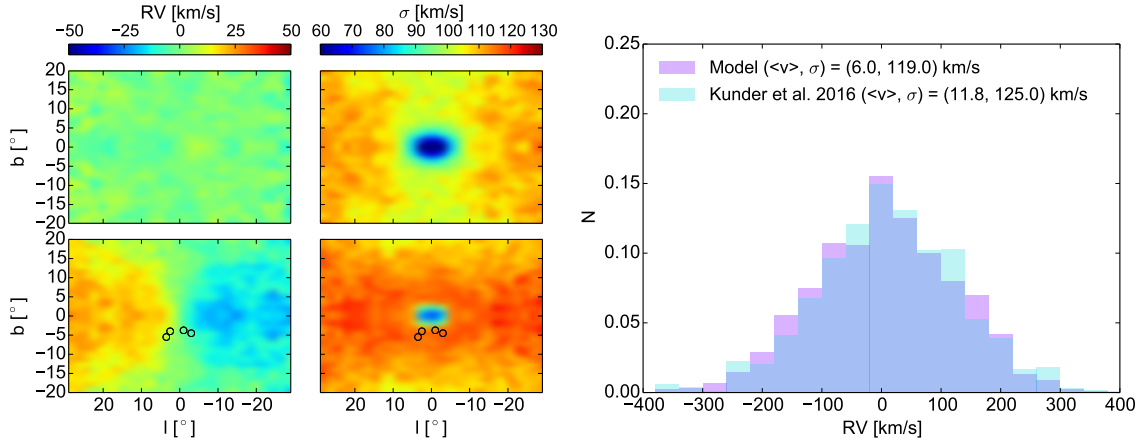


Figure 3. *Left:* Kinematic maps of the mean radial velocity (RV) and velocity dispersion at $t = 0$ (top) and at the final time (bottom). *Right:* RV distribution in four bulge fields for RR Lyrae stars from Kunder et al. (2016) compared with our stellar halo model. The four fields are shown as circles in the lower kinematic maps on the left.

Notice that bar-following particles have faster rotation (~ 80 km/s) than the not-bar-following particles, but also that the relative contribution of the bar-following particles is concentrated in the inner bulge region and is very small elsewhere. We also see in Figure 4 a counterrotating structure for the not-bar-following particles (third middle panel). A possible reason for the presence of this structure is that the bar traps prograde orbits more easily than retrograde orbits.

Figure 5 is similar to Figure 4 but shows (x, y) and (x, z) projections rather than (l, b) . With this Figure we point out that the bar-following particles do not show an X-shaped structure as is observed for stars in the B/P bulge, and that the bar-following orbits dominate only in the inner few degrees where even their rotation is small, and that their contribution elsewhere is also small.

6 CONCLUSIONS

We constructed a model for the old stellar halo in the Milky Way (MW) as traced by RR Lyrae (RRL) stars in order to investigate the origin of the triaxial shape and slow rotation of RRL in the bulge region. Based on observational constraints, we assumed an oblate shape with a single power-law density ($\rho \propto m^{-3}$) at early times. Using an N-body simulation for the MW, we followed the evolution of this stellar halo component until several Gyr after formation of the Galactic bar and B/P bulge. With this model, we addressed the effect of the bar and B/P bulge on the MW's inner metal-poor halo, and made predictions for its density distribution and kinematics. Our main conclusions can be summarized as follows:

- The extrapolated density profile of RRLs in the bulge, with power-law index of $\simeq -3$, approximately agrees with the RRL density profiles in the stellar halo at $5 - 20$ kpc.
- Through the gravitational influence of the Galactic bar and B/P bulge during their formation and evolution, the shape of the inner stellar halo evolves from oblate to triaxial.
- Our model predicts a slow mean radial velocity in approximate agreement with recent measurements at $l \sim 4^\circ$,

rising to $\sim 15 - 25$ km/s at $l = 10^\circ - 30^\circ$, and a velocity dispersion of ~ 120 km/s. This rotation measured in the later stages of the N-body simulation is due to the angular momentum transfer during the bar evolution.

- With frequency analysis we separated the stellar halo particles into bar-following and not-bar-following orbits, and found that bar-following orbits are a minority, $\sim 12\%$ of all orbits within 5 kpc. This is the reason for the slow rotation in our halo model.

- The old component traced by RRLs in the bulge could be the inner extension of the Galactic stellar halo. It does not participate in the X-shape structure.

ACKNOWLEDGMENTS

We thank Christopher Wegg for helpful discussions. APV acknowledges the support of a postdoctoral fellowship of CONACyT.

REFERENCES

- Akhter, S., Da Costa, G. S., Keller, S. C., & Schmidt, B. P. 2012, *ApJ*, 756, 23
- Alcock, C., Allsman, R. A., Alves, D. R., et al. 1998, *ApJ*, 492, 190
- Amrose, S., & McKay, T. 2001, *ApJ*, 560, L151
- Athanassoula, E., & Misiriotis, A. 2002, *MNRAS*, 330, 35
- Babusiaux, C., Gómez, A., Hill, V., et al. 2010, *A&A*, 519, A77
- Chen, B., Stoughton, C., Smith, J. A., et al. 2001, *ApJ*, 553, 184
- Combes, F., Debbasch, F., Friedli, D., & Pfenniger, D. 1990, *A&A*, 233, 82
- Debattista, V. P., Mayer, L., Carollo, C. M., et al. 2006, *ApJ*, 645, 209
- Dékány, I., Minniti, D., Catelan, M., et al. 2013, *ApJ*, 776, L19
- de Lorenzi, F., Debattista, V. P., Gerhard, O., & Sambhus, N. 2007, *MNRAS*, 376, 71
- For, B.-Q., Sneden, C., & Preston, G. W. 2011, *ApJS*, 197, 29
- Fux, R. 1997, *A&A*, 327, 983
- Gonzalez, O. A., Zoccali, M., Vasquez, S., et al. 2015, *A&A*, 584, A46

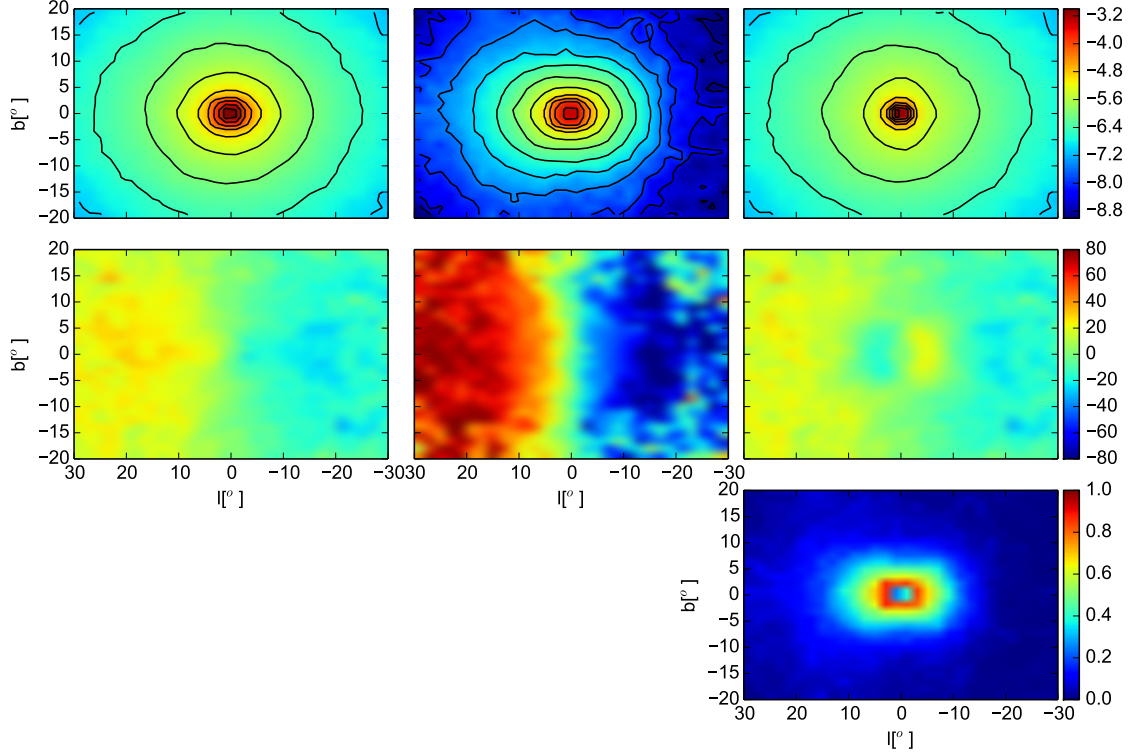


Figure 4. *Top:* Surface density distribution for the entire sample of 30000 stellar halo particles, for the bar-following halo particles, and the not-bar-following particles, from left to right (logarithmic scale). *Middle:* Radial velocity map for the entire sample, for the bar-following particles, and for the not bar-following particles, from left to right (in km/s). *Bottom:* Relative contribution of the bar-following halo particles.

Hill, V., Lecureur, A., Gómez, A., et al. 2011, *A&A*, 534, A80
 Jurić, M., Ivezić, Ž., Brooks, A., et al. 2008, *ApJ*, 673, 864
 Jurcsik, J., & Kovacs, G. 1996, *A&A*, 312, 111
 Keller, S. C., Murphy, S., Prior, S., Da Costa, G., & Schmidt, B. 2008, *ApJ*, 678, 851
 Kunder, A., Rich, R. M., Koch, A., et al. 2016, *ApJ*, 821, L25
 Martinez-Valpuesta, I., & Gerhard, O. 2011, *ApJ*, 734, L20
 Minniti, D., Alcock, C., Allsman, R. A., et al. 1999, *The Third Stromlo Symposium: The Galactic Halo*, 165, 284
 Morrison, H. L., Mateo, M., Olszewski, E. W., et al. 2000, *AJ*, 119, 2254
 Nemec, J. M., Cohen, J. G., Ripepi, V., et al. 2013, *ApJ*, 773, 181
 Ness, M., Freeman, K., Athanassoula, E., et al. 2013a, *MNRAS*, 430, 836
 Ness, M., Freeman, K., Athanassoula, E., et al. 2013b, *MNRAS*, 432, 2092
 Nissen, P. E., & Schuster, W. J. 2010, *A&A*, 511, L10
 Phleps, S., Drepper, S., Meisenheimer, K., & Fuchs, B. 2005, *A&A*, 443, 929
 Pietrukowicz, P., Udalski, A., Soszyński, I., et al. 2012, *ApJ*, 750, 169
 Pietrukowicz, P., Kozłowski, S., Skowron, J., et al. 2015, *ApJ*, 811, 113
 Portail, M., Wegg, C., Gerhard, O., & Martinez-Valpuesta, I. 2015, *MNRAS*, 448, 713
 Portail, M., Wegg, C., & Gerhard, O. 2015, *MNRAS*, 450, L66
 Rich, R. M. 1988, *AJ*, 95, 828
 Rojas-Arriagada, A., Recio-Blanco, A., Hill, V., et al. 2014, *A&A*, 569, A103
 Saha, K., Martinez-Valpuesta, I., & Gerhard, O. 2012, *MNRAS*, 421, 333

Sesar, B., Ivezić, Ž., Stuart, J. S., et al. 2013, *AJ*, 146, 21
 Sevenster, M., Saha, P., Valls-Gabaud, D., & Fux, R. 1999, *MNRAS*, 307, 584
 Shen, J., Rich, R. M., Kormendy, J., et al. 2010, *ApJ*, 720, L72
 Siegel, M. H., Majewski, S. R., Reid, I. N., & Thompson, I. B. 2002, *ApJ*, 578, 151
 Soszyński, I., Dziembowski, W. A., Udalski, A., et al. 2011, *Acta Astron.*, 61, 1
 Soszyński, I., Udalski, A., Szymański, M. K., et al. 2014, *Acta Astron.*, 64, 177
 Syer, D., & Tremaine, S. 1996, *MNRAS*, 282, 223
 Torrealba, G., Catelan, M., Drake, A. J., et al. 2015, *MNRAS*, 446, 2251
 Vivas, A. K., & Zinn, R. 2006, *AJ*, 132, 714
 Walker, A. R., & Terndrup, D. M. 1991, *ApJ*, 378, 119
 Wegg C., Gerhard O., 2013, *MNRAS*, 435, 1874
 Wetterer, C. J., & McGraw, J. T. 1996, *AJ*, 112, 1046
 Zoccali, M., Renzini, A., Ortolani, S., et al. 2003, *A&A*, 399, 931

This paper has been typeset from a \LaTeX file prepared by the author.

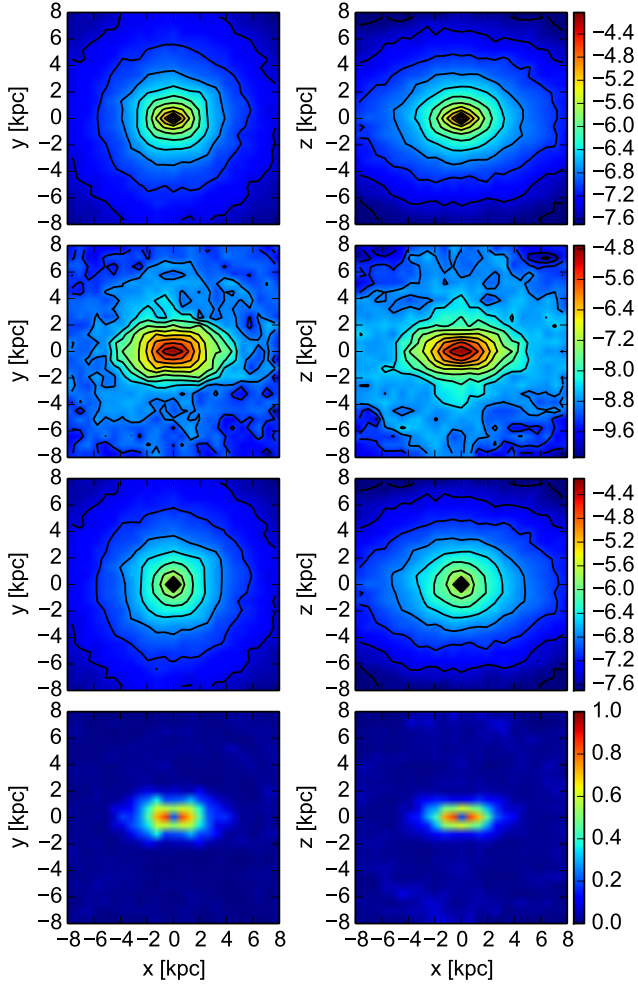


Figure 5. Face-on (left panels) and side-on (right panels) surface density projections for the entire sample of 30000 (first row), the bar-following particles (second row), and the not-bar-following particles (third row; logarithmic scale). The bottom panels show the relative contributions of the bar-following halo particles in the face-on and side-on projections.